

Spatial and temporal variability of $p\text{CO}_2$ and CO_2 emissions from the Dongjiang River in South China

Boyi Liu¹, Mingyang Tian², Kaimin Shih³, Chun Ngai Chan¹, Xiankun Yang⁴, Lishan Ran¹

5 ¹Department of Geography, the University of Hong Kong, Hong Kong SAR, China

²Institute for Geology, Center for Earth System Research and Sustainability (CEN), Universität Hamburg, Hamburg, Germany

³Department of Civil Engineering, the University of Hong Kong, Hong Kong SAR, China

⁴School of Geographical Sciences, Guangzhou University, Guangzhou, 510006, China

10

Correspondence to: Lishan Ran (lsran@hku.hk)

Abstract. CO_2 efflux at the water–air interface is an essential component of the riverine carbon cycle. However, the lack of spatially resolved CO_2 emission measurement still hinges the accuracy of estimates on global riverine CO_2 emissions. By deploying floating chambers, seasonal changes in river water CO_2 partial pressure ($p\text{CO}_2$) and CO_2 evasion from the Dongjiang River in South China were investigated. Spatial and temporal patterns of $p\text{CO}_2$ were mainly affected by terrestrial carbon inputs and in-stream metabolism, both of which varied due to differential catchment settings, land cover, and hydrological conditions. Temperature-normalized gas transfer velocity (k_{600}) in small rivers were $8.29 \pm 11.29 \text{ m d}^{-1}$ and $4.90 \pm 3.82 \text{ m d}^{-1}$ for the wet season and dry season, respectively, which were nearly 70 % higher than that of large rivers ($3.90 \pm 5.55 \text{ m d}^{-1}$ during the wet season and $2.25 \pm 1.61 \text{ m d}^{-1}$ during the dry season). A significant correlation was observed between k_{600} and flow velocity but not wind speed regardless of river size. Majority of the surveyed rivers were net CO_2 source while exhibiting substantial seasonal variations. The mean CO_2 flux was 300.1 and $264.2 \text{ mmol m}^{-2} \text{ d}^{-1}$ during the wet season for large and small rivers, respectively, 2-fold larger than that during the dry season. However, no significant difference in CO_2 flux was observed between small and large rivers. The absence of commonly observed higher CO_2 fluxes in small rivers could be associated with the depletion effect caused by abundant and consistent precipitation in this subtropical monsoon catchment.

15
20
25

1 Introduction

River networks act as a processor that transfers and emits the carbon entering the water, rather than just
30 a passive pipe that transports carbon from the terrestrial ecosystem to the ocean (Cole et al., 2007; Battin
et al., 2009; Drake et al., 2018). CO₂ emissions at the water–air interface are an essential component of
the riverine carbon cycle. CO₂ emitted from inland waters to the atmosphere reaches up to 2.9 PgC yr⁻¹,
surpassing that transported from land to ocean through rivers (Sawakuchi et al., 2017; Drake et al., 2018).
Understanding the role that rivers play in the global carbon cycle is still hindered by uncertainty on the
35 estimate of CO₂ flux outgassing from rivers (Cole et al., 2007; Raymond et al., 2013; Sawakuchi et al.,
2017; Drake et al., 2018). Riverine carbon emissions have significant temporal and spatial variations,
making it challenging to quantify carbon emissions accurately. In addition, watershed geomorphology,
hydrological conditions, climate, and other environmental factors can affect the CO₂ efflux in rivers (Alin
et al., 2011; Abril et al., 2014; Almeida et al., 2017; Ran et al., 2017a; Borges et al., 2018). Thus, there
40 are substantial differences in CO₂ efflux among rivers in different climate regions, or the same river but
between different seasons (Denfeld et al., 2013; Rasera et al., 2013). An enhanced understanding of the
temporal and spatial characteristics of the water–air CO₂ flux will facilitate a more robust estimate.
However, global riverine carbon emission estimates were largely based on data disproportionately
focusing on temperate and boreal regions, including North America and Europe (Raymond et al., 2013;
45 Lauerwald et al., 2015; Drake et al., 2018). In light of this data gap, more studies are required in other
data-poor regions to achieve a more accurate estimate.

Rivers in tropical and subtropical regions of East Asia and Southeast Asia are among those
underrepresented regions that need more attention since they are essential participants in riverine carbon
transport (Ran et al., 2015; Ran et al., 2017b; Drake et al., 2018). The high temperature in this region
50 facilitated a high net primary productivity in the terrestrial ecosystem and intense biochemical activities,
and both contributed to the carbon input dynamic from soil to rivers (Li et al., 2018). Meanwhile, rivers
in this region are under the heavy influence of monsoon, and riverine CO₂ emissions vary significantly
among seasons due to the changes in temperature and precipitation. In addition, different rivers in this
region may have contrasting trends in CO₂ dynamic due to different underlying controlling factors. Some
55 rivers have the highest CO₂ efflux in the wet season (Li et al., 2013; Le et al., 2018; Ni et al., 2019),
while others have the highest CO₂ efflux in the dry season (Luo et al., 2019), suggesting that an increase
in wet season runoff can have two distinct consequences. One possibility is that it increases external

carbon inputs and CO₂ emissions (Hope et al., 2004; Johnson et al., 2008), while the other is that it leads to a dilution of CO₂ in rivers and accordingly a reduction in CO₂ emissions (Ran et al., 2017b; Li et al., 60 2018). Since starkly different outcomes can occur, it is important to investigate the processes behind such diverse response of rivers to the monsoon.

The Dongjiang River (DJR), located in the subtropical region of South China, is one of the three tributaries of the Pearl River. Previous studies on riverine carbon transportation and emissions in the Pearl rivers mainly focused on the Xijiang River, which was characterized by widely distributed 65 carbonate rocks, and the estuary area of the Pearl River Delta (Yao et al., 2007; Zhang et al., 2015; Zhang et al., 2019; Liang et al., 2020). Though some studies have been conducted in the Dongjiang River basin (DJRB) focusing on carbon transport and the carbon sink effect of chemical weathering (Tao et al., 2011; Fu et al., 2014), there is still a lack of understanding of the characteristics of catchment-wide CO₂ emissions in DJRB. Furthermore, a predominantly hilly landscape combined with abundant precipitation 70 favors the formation of a great number of small rivers in DJRB (Ding et al., 2015). However, the current estimate of basin-wide CO₂ emission from the river network was mostly based on the data from large rivers, and small rivers are heavily underrepresented (Raymond et al., 2013; Drake et al., 2018). Because the controlling factors and the input of carbon could be significantly different between large and small rivers (Johnson et al., 2008; Dinsmore et al., 2013; Hotchkiss et al., 2015; Marx et al., 2017), which can 75 lead to very distinctive pattern of carbon dioxide evasion, more comprehensive quantification of CO₂ evasion from small headwater streams is necessary. Therefore, studies on the characteristics of riverine CO₂ emission in DJRB should be conducted among river size spectrums, and the impact of monsoon ought to be considered.

By using directly measured river water CO₂ partial pressure ($p\text{CO}_2$) and CO₂ efflux data from DJRB, and 80 in conjunction with hydrological and physicochemical data, the objectives of this study were to 1) investigate the spatial and temporal pattern of $p\text{CO}_2$ and CO₂ emission along stream size spectrum, 2) examine the differences in hydrological and physicochemical controls of $p\text{CO}_2$ and the CO₂ evasion between small headwater streams and large rivers. The results of this study could shed light on the underlying controls of the spatial and temporal distribution of riverine $p\text{CO}_2$ and support a refined 85 estimate of regional and global carbon budgets.

2 Material and methods

2.1 Site Description

The DJR in South China is one of the three major tributaries of the Pearl River system (Figure 1). It has a 562 km long mainstem channel and a drainage area of 35,340 km² (Chen et al., 2011). Due to its
90 subtropical monsoon climate, precipitation in DJRB exhibits significant seasonal variability (Figure 2a).
The multi-annual average precipitation is about 1800 mm, 80 % of which is concentrated during the wet
season from April to September. The Boluo Hydrological Gauge is the lowermost gauge of the Dongjiang
River mainstem channel, controlling a drainage area of ~23,000 km². The multi-annual average water
discharge at Boluo Hydrological Gauge is 23.7 km³ (Zhang et al., 2008). About 80–90 % of this discharge
95 is transported during the wet season (Figure 2b). The landscape is characterized by plains and hills,
accounting for 87.3 % of the river basin area (Ding et al., 2015), and the dominant land use of the
catchment is highly diverse evergreen forests of broad-leaved and needle-leaved species (Ran et al., 2012;
Chen et al., 2013). The impacts of human activities on land use vary among three regions in the DJRB.
Urban expansion and agricultural activities have substantially altered the land use in Lower and Middle
100 Dongjiang River Basin (LDJRB and MDJRB), respectively, while the Upper Dongjiang River Basin
(UDJRB) is less affected by human activities (Figure 1).

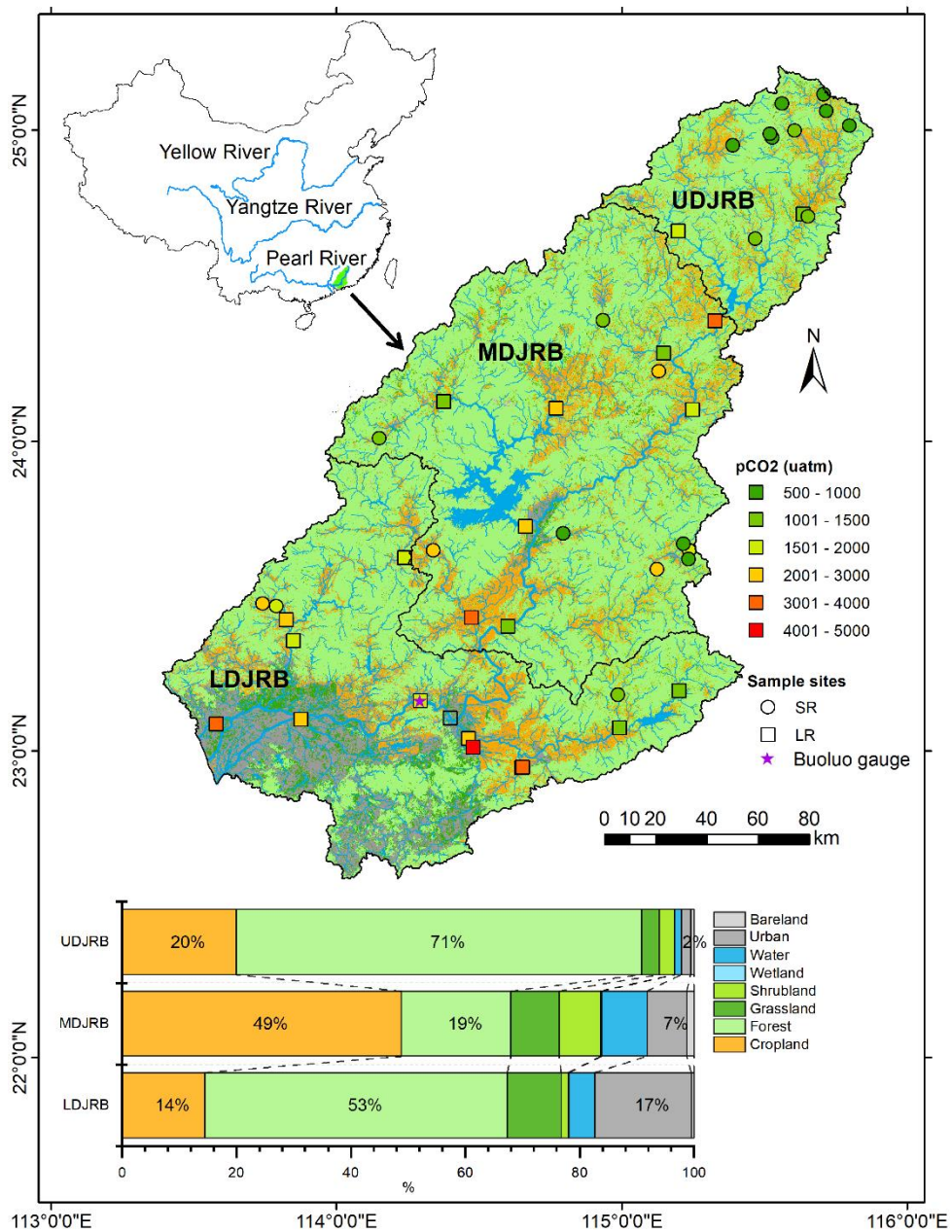
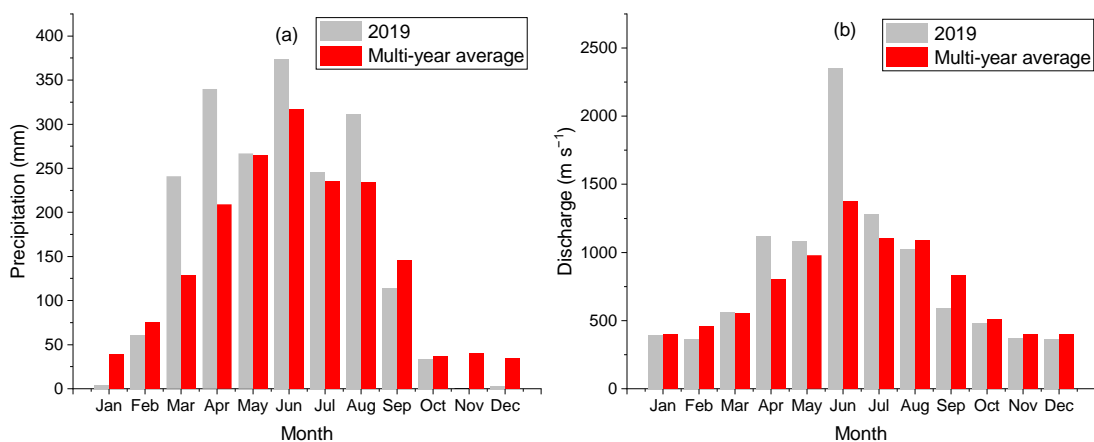


Figure 1 Sample sites and land cover in the DJRB. Yearly average $p\text{CO}_2$ at each sample site was displayed. Based on land cover dataset: FROM-GLC10 (<http://data.ess.tsinghua.edu.cn>).



105

Figure 2 Monthly variations in (a) precipitation of the DJRB and (b) water discharge at the Boluo hydrological gauge, based on data provided by the Hydrological Bureau of Guangdong Province.

2.2 Field Measurement and Analysis

In total, there were 43 sampling sites spanning seven Strahler stream orders. Fourth to seven order
 110 streams were mainstem and major tributaries, while first to third order streams were small tributaries. River widths were measured by a laser rangefinder. Sampled rivers were categorized, according to their stream orders, into small rivers (first to third order streams, SR) and large rivers (fourth to seventh order streams, LR). The small rivers had an average width of 15.4 ± 10.2 m, while large rivers have an average width of 180.3 ± 159.3 m (Table S1). Those sampling sites were widely distributed in the mainstem and
 115 nine major subcatchments among three regions with different topographic features and land cover (Figure 1). In order to investigate CO₂ emissions during different hydrological conditions, we performed five fieldwork campaigns from December 2018 to October 2019, including three in the wet season (early wet season - late April, middle wet season - early July, and late wet season - late August) and two in the dry season (middle dry season - December 2018 to early January 2019 and early dry season - late October
 120 2019. Sample sites were measured in the daytime over two weeks for each field trip. Three rounds of campaigns in the wet season allow each sample site to be measured under different hydrological conditions, and the two-week duration of each campaign allowed streams with different orders and sizes to be measured under various discharges. As for the dry season, the hydrological condition was relatively stable due to low precipitation. However, field measurements conducted during the daytime could lead
 125 to an underestimate in $p\text{CO}_2$ and CO₂ emission (Reiman and Xu, 2019a). Nocturnal CO₂ emission rates

in rivers could be 27% greater than the daytime rates (Gómez-Gener et al., 2021). During the field trips, water temperature, pH, and dissolved oxygen (DO) were measured with a portable multiparameter probe (Multi 3430, WTW GmbH, Germany). The pH probe was calibrated before each field trip with standard pH buffers (4.01 and 7.00). Measurements were conducted 10 cm below the water surface. To evaluate
130 the contribution of metabolism on DO changes, ΔCO_2 and ΔO_2 were calculated as described by Stets et al. (2017) using:

$$\Delta\text{CO}_2 = \text{CO}_{2w} - \text{CO}_{2a} \quad (1)$$

and

$$\Delta\text{O}_2 = \text{O}_{2w} - \text{O}_{2a} \quad (2)$$

135 Where CO_{2w} and O_{2w} are measured concentrations of CO_2 and O_2 in water sample, while CO_{2a} and O_{2a} are the equilibrium CO_2 and O_2 concentrations ($\mu\text{mol L}^{-1}$).

Flow velocity was determined by using a Global Water Flow Probe FP111 with a precision of 0.1 m s^{-1} , while wind speed at 1.5 m above the water surface was measured with a Kestrel 2500 handheld anemometer and normalized to a height of 10 m (U10) using the equation from Alin et al. (2011). As the
140 flow velocity was measured near the riverbanks, an underestimation of the flow velocity is possible. Flow velocity measured near the riverbanks is only about 40% of the maximum flow velocity at the cross-section (Moramarco et al., 2004; Le Coz et al., 2008). We also collected water for analyzing total alkalinity (TA) and dissolved organic carbon (DOC). Firstly, 100 ml of water samples were filtered through a pre-combusted glass fiber filter (pore size: $0.47 \mu\text{m}$, Whatman GF/F, GE Healthcare Life
145 Sciences, USA). Then, 50 ml of water used for TA analysis was titrated with 0.1 mol L^{-1} HCl on the same day of sampling. The remaining 50 ml of water for DOC analysis was poisoned with concentrated H_2SO_4 to $\text{pH} < 2$ and preserved in a cooler with ice bags before analysis. DOC was determined by the high-temperature combustion method using a TOC Analyzer (Elementar Analysensysteme GmbH, Langenselbold, Germany) that has a precision better than 3 %.

150 **2.3 Calculation of $p\text{CO}_2$ and CO_2 emission flux**

The surface water $p\text{CO}_2$ was determined using the headspace equilibrium method, which could avoid the possible overestimation of using TA and pH to calculate $p\text{CO}_2$ in rivers with a relatively low pH (Abril et al., 2015). We used a 625 mL reagent bottle to collect 400 mL of water from ~10 cm below the surface,

leaving 225 mL of space filled with ambient air as headspace. The bottle was then immediately capped
 155 and shaken vigorously for at least 1 min to achieve an equilibrium between the water and the CO₂ in the
 headspace (Hope et al., 1994). Then, the bottle was connected to the calibrated Li-850 CO₂/H₂O gas
 analyzer (Li-Cor, Inc, USA), and the equilibrated gas in this closed loop was measured. The
 measurements at each site were repeated twice, and the average was then calculated. The variation
 between the two measurements was less than 5%, and the accuracy of Li-850 is within 1.5% of the
 160 reading. The ambient air pCO_2 (pCO_2^{air}) was measured before the headspace measurements and the
 chamber deployments. The pCO_2^{air} value varied between 380 and 450 μatm . The original surface water
 pCO_2 ($pCO_2^{water,i}$) was finally calculated by using solubility constants (K_0) for CO₂ from Weiss (1974),
 Carbonate constants (K_1 , K_2) from (Millero et al., 2006), and the volume of the flask, headspace, and
 residual system (line and gas analyzer) (Dickson et al., 2007; Ran et al., 2017a; Tian et al., 2019) using:

$$165 \quad pCO_2^{water,i} = pCO_2^{headspace,f} + \left(\frac{V_h + V_r}{V_w}\right)(pCO_2^{h+r} - pCO_2^{headspace,i}) / [RTK_0(1 + \frac{K_1}{[H^+]} + \frac{K_1K_2}{[H^+]^2})] \quad (3)$$

Where V_h , V_r and V_w , are the headspace volume, residence system volume, and water volume,
 respectively. R is the universal gas constant ($8.314 \text{ J mol}^{-1} \text{ K}^{-1}$), T is the water temperature in Kelvin
 (K), and $[H^+]$ is the concentration of hydrogen ion. $pCO_2^{headspace,i}$ and $pCO_2^{headspace,f}$ are pCO_2 before
 and after the headspace equilibration, respectively. pCO_2^{h+r} is the pCO_2 of the mixed gas in the headspace
 170 and residual system during the measurement. the $pCO_2^{headspace,i}$ was taken as the pCO_2 in ambient air
 before the measurement, while $pCO_2^{headspace,f}$ was calculated using:

$$pCO_2^{headspace,f} = pCO_2^{h+r} + \left(\frac{V_r}{V_h}\right)(pCO_2^{h+r} - pCO_2^{headspace,i}) \quad (4)$$

For measuring V_r , We filled the headspace with gas, which had a known pCO_2 , and measured the pCO_2
 in the closed loop. V_r was then estimated according to equation (3). A comparative analysis of the syringe
 175 and bottle headspace method has been conducted to evaluate the accuracy of the headspace extraction
 method used in this study (Table S2 and Figure S2). Overall, our method could cause a 1–5%
 underestimation in pCO_2 .

To reduce the artificial turbulence induced by anchored chambers, we used a small unmanned boat in the
 measurement, which allowed us to deploy drifting chambers freely in rivers deeper than 0.2 m and with
 180 a high flow velocity up to 2 m s^{-1} . During the deployment, CO₂ emission was determined using a circular,

8.5 L floating chamber with a water surface area of 0.113 m². The chamber walls were lowered about 2 cm into the water and mounted with a pneumatic rubber tire. The chamber was connected to an infrared Li-850 CO₂/H₂O gas analyzer (Li-Cor, Inc, USA) in a floating storage box through Polyurethane tubes for CO₂ analysis. An unmanned boat connected to both the chamber and box with ropes was used to
 185 deploy them near the central line of the river. Once the entire setup reached its designated location, the readings on the Li-850 were recorded at 0.5 s intervals. During the entire measurement process, the box drifted freely with the current. The Li-850 was calibrated by the manufacturer before field trips. The rate of CO₂ efflux (FCO₂ in mmol m⁻² d⁻¹) was calculated from the observed change rate of the mole fraction S (ppm s⁻¹) using:

$$190 \quad FCO_2 = (S \cdot V / A) \cdot t_1 \cdot t_2 \quad (5)$$

Where S is the slope of CO₂ accumulation in the chamber (μatm s⁻¹), V is chamber gas volume (m³), A is the chamber area (m²), t₁ = 8.64 · 10⁴ s d⁻¹ is the conversion factor from seconds to days, and t₂ is a conversion factor from mole fraction (ppm) to concentration (mmol m⁻³) at in situ temperature (T in K) and atmospheric pressure (p in Pa), according to the ideal gas law:

$$195 \quad t_2 = p / (8.31 JK^{-1} \text{mole}^{-1} \cdot T) \cdot 1000 \quad (6)$$

The gas transfer velocity (*k*) was calculated from FCO₂ and *p*CO₂ in both water and ambient air using:

$$k = FCO_2 / (K_0 \cdot (pCO_2^{water,i} - pCO_2^{air})) \quad (7)$$

To compare gas transfer velocity values among different sites, *k* was standardized to *k*₆₀₀ as described by Alin et al. (2011) using:

$$200 \quad k_{600} = k(600/Sc)^{-0.5} \quad (8)$$

Where, *Sc* is the Schmidt number, which is dependent on temperature (T) in degree Celsius (Wanninkhof, 1992):

$$Sc = 1911.1 - 118.11T + 3.4527T^2 - 0.4132T^3 \quad (9)$$

In total, 196 chamber measurements were made. In 19 out of 215 sample sites, the drifting chamber was
 205 unable to deploy due to shallow water or high flow velocity. Meanwhile, 8 out of 196 *k*₆₀₀ data with the

air–water $p\text{CO}_2$ gradient less than 200 μatm were also excluded, as the error in these calculations could be considerable (Borges et al., 2004).

3 Result

3.1 Physical and Biochemical Characteristics

210 The Dongjiang River was characterized by substantial seasonal variations in hydrologic regimes (Figure
2). Stream width in the wet season was 17.0 % and 5.6 % larger than that in the dry season for small and
large rivers, respectively (Table S1). The discharge ranged 4 orders of magnitude from 0. 1 $\text{m}^3 \text{s}^{-1}$ in the
small headwater streams during the dry season to 6690 $\text{m}^3 \text{s}^{-1}$ in the main stem during the wet season
(Figure S1). Water temperature was higher in July and August (21.4–33 and 21–33.4 °C, respectively)
215 than that in January (8.1–22.2 °C), April (16.5–26.9 °C), and October (17.4–29.7 °C). pH varied from
6.38 to 8.14, with a mean of 7.08. There was no significant (independent sample t test, $p > 0.05$) change
in pH between wet and dry seasons. U10 based on all stream sites was higher in large rivers (0.86 ± 0.91
and $1.43 \pm 1.58 \text{ m s}^{-1}$ in wet and dry season, respectively) than in small rivers (0.62 ± 0.61 and $0.76 \pm$
 0.73 m s^{-1} in wet and dry season, respectively).

220 The streams presented low alkalinity ranging from 225 to 3025 $\mu\text{mol L}^{-1}$. Overall, lower alkalinity was
observed in wet season than in dry season (Table 1). In small rivers, the alkalinity in wet season ($656 \pm$
 $265 \mu\text{mol L}^{-1}$) was 21.1 % lower than the dry season ($831 \pm 460 \mu\text{mol L}^{-1}$), and the lowest alkalinity was
observed in April ($615 \pm 262 \mu\text{mol L}^{-1}$), which was 30.4 % lower than in January ($883 \pm 548 \mu\text{mol L}^{-1}$).
Similarly, the alkalinity in large rivers was $790 \pm 402 \mu\text{mol L}^{-1}$ in wet season, 14.5 % lower than $924 \pm$
225 $411 \mu\text{mol L}^{-1}$ in dry season. However, the lowest value of alkalinity in large rivers was observed in
August ($739 \pm 312 \mu\text{mol L}^{-1}$) instead of April in small rivers.

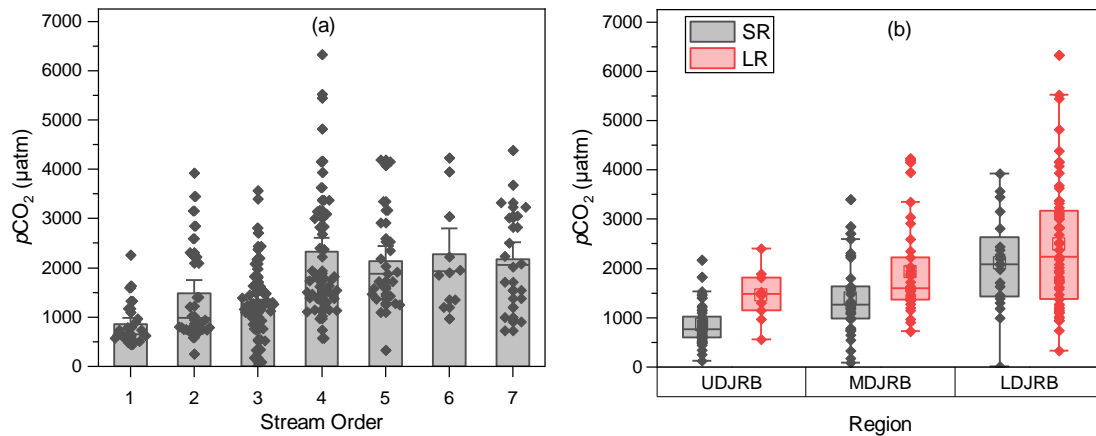
Spatial and seasonal changes in DOC concentration were also observed in the surveyed rivers (Table
1). DOC concentration in larges rivers ($1.94 \pm 1.52 \text{ mg L}^{-1}$) was 41.6 % higher than that in small rivers
($1.37 \pm 0.72 \text{ mg L}^{-1}$). Meanwhile, DOC concentrations in the wet season were $2.22 \pm 1.82 \text{ mg L}^{-1}$ and
230 $1.54 \pm 0.72 \text{ mg L}^{-1}$ for large and small rivers, respectively, which were 45.1 % and 54 % higher than
that in the dry season (1.53 ± 0.72 and $1.11 \pm 0.63 \text{ mg L}^{-1}$ for large and small rivers, respectively).

Table 1 Seasonal Variations of Physical and Biochemical Characteristics, expressed as Mean \pm SD.

Stream size	Season	Month	Water Temperature (°C)	pH	Alkalinity ($\mu\text{mol L}^{-1}$)	DOC (mg L^{-1})
<i>small</i>	Dry	January	14.3 \pm 4.1	7.05 \pm 0.31	883 \pm 548	1.07 \pm 0.37
	Wet	April	19.9 \pm 1.9	7.19 \pm 0.26	615 \pm 262	1.51 \pm 0.58
	Wet	July	25.7 \pm 2.3	7.17 \pm 0.27	676 \pm 227	1.59 \pm 0.97
	Wet	August	27.1 \pm 3.0	7.13 \pm 0.38	678 \pm 308	1.51 \pm 0.56
	Dry	October	21.5 \pm 2.6	7.08 \pm 0.23	778 \pm 358	1.16 \pm 0.82
<i>large</i>	Dry	January	16.9 \pm 5.5	7.00 \pm 0.27	961 \pm 409	1.70 \pm 1.52
	Wet	April	22.1 \pm 3.7	7.20 \pm 0.27	890 \pm 386	2.22 \pm 1.65
	Wet	July	27.8 \pm 2.9	6.92 \pm 0.25	740 \pm 305	1.97 \pm 1.77
	Wet	August	28.9 \pm 3.3	6.92 \pm 0.26	739 \pm 312	2.47 \pm 2.04
	Dry	October	25.2 \pm 3.1	7.13 \pm 0.29	887 \pm 331	1.37 \pm 0.67

3.2 Spatial and Seasonal variation in $p\text{CO}_2$

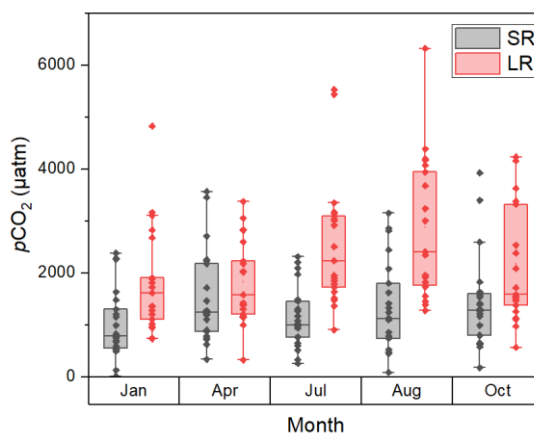
The $p\text{CO}_2$ ranged from 15 to 6323 μatm with a catchment-wide average of 1748 μatm and showed considerable temporal and spatial variation throughout the sampling period. There was an increasing trend of observed $p\text{CO}_2$ from small to large rivers (Figure 3a). On average, the $p\text{CO}_2$ values were 856 \pm 444, 1481 \pm 979, 1354 \pm 753, 2332 \pm 1330, 2142 \pm 1016, 2271 \pm 1121, and 2168 \pm 1046 μatm for streams from first to seventh order, respectively. The stronger increase in $p\text{CO}_2$ occurred between third and fourth order streams (from 1354 \pm 753 to 2332 \pm 1330 μatm , Figure 3a). Overall, $p\text{CO}_2$ in large rivers (2250 \pm 1178 μatm) was 76.3 % higher than that in small rivers (1276 \pm 796 μatm). Meanwhile, there was also an increasing trend of $p\text{CO}_2$ from rivers in UDJRB to those in LDJRB. The $p\text{CO}_2$ values were 2105 \pm 959 and 2487 \pm 1276 μatm for small and large rivers respectively in LDJRB, which were 146.7% and 70% higher than that in UDJRB, respectively (Figure 3b).



245 **Figure 3** Spatial variations in $p\text{CO}_2$. (a) Yearly average $p\text{CO}_2$ in the seven stream orders, standard errors (SE) are displayed by error bars. (b) Measured $p\text{CO}_2$ in small and large rivers among three regions in the DJRB. The box mid-lines represent medians; the interquartile range (IQR) is represented by top and bottom of the box, respectively; whiskers indicate the range of 1.5 IQR; the white square symbols represent means, and the other symbols represent $p\text{CO}_2$ values for each sampled site.

250 Seasonal variations of $p\text{CO}_2$ differ across the stream size spectrum (Figure 4). In small rivers, the highest $p\text{CO}_2$ was observed in April ($1506 \pm 880 \mu\text{atm}$), which was 50.3 % higher compared with January ($1002 \pm 660 \mu\text{atm}$). $p\text{CO}_2$ then decreased in July ($1131 \pm 589 \mu\text{atm}$) and increased in August ($1325 \pm 863 \mu\text{atm}$) and October ($1414 \pm 900 \mu\text{atm}$). Compared with small rivers, the peak of $p\text{CO}_2$ in large rivers occurred later but persisted for a longer period of time. In large rivers, an increase in $p\text{CO}_2$ was not observed until

255 July. $p\text{CO}_2$ in April was $1831 \pm 793 \mu\text{atm}$, which was similar to $1805 \pm 1010 \mu\text{atm}$ in January, and it increased 39.3 % to $2550 \pm 1210 \mu\text{atm}$ in July. $p\text{CO}_2$ peaked in August ($2885 \pm 1351 \mu\text{atm}$) and then decreased to 2176 ± 1166 in October. Overall, $p\text{CO}_2$ was 9.3 % and 21.7 % higher in wet season than in dry season for small and large rivers, respectively.



260 **Figure 4** Seasonal $p\text{CO}_2$ in small and large rivers. The box mid-lines represent medians; the interquartile range (IQR) is represented by top and bottom of the box, respectively; whiskers indicate the range of 1.5 IQR; the white square symbols represent means, and the other symbols represent $p\text{CO}_2$ values for each sampled site.

3.3 CO_2 effluxes and k_{600}

265 CO_2 effluxes ranged from -129.8 to $3874.8 \text{ mmol m}^{-2} \text{ d}^{-1}$ with a mean of $225.2 \text{ mmol m}^{-2} \text{ d}^{-1}$. More than 95 % of the 196 samples had positive FCO_2 values, indicating that the majority of the surveyed rivers is a carbon source. Overall, we observed higher FCO_2 during wet season than during dry season in both small and large rivers (Figure 5a). FCO_2 in small rivers and large rivers were 264.2 ± 410.0 and $300.1 \pm 511.7 \text{ mmol m}^{-2} \text{ d}^{-1}$ respectively during the wet season, which was 87.2 % and 123.1 % higher than that in the dry season (141.1 ± 188.7 and $134.5 \pm 129.5 \text{ mmol m}^{-2} \text{ d}^{-1}$ for small and large rivers respectively).

270 No significant (independent sample t test, $p > 0.05$) difference in FCO_2 was observed between small and large rivers.

k_{600} differs greatly between river size classes and among hydrological periods (Figure 5b). k_{600} values in small rivers were significantly (independent sample t test, $p < 0.001$) higher on average than in large rivers. The mean values of k_{600} in small rivers were $8.29 \pm 11.29 \text{ m d}^{-1}$ and $4.90 \pm 3.82 \text{ m d}^{-1}$ for the wet season and dry season, respectively, which were 112.6 % and 70 % higher than that of large rivers ($3.90 \pm 5.55 \text{ m d}^{-1}$ in the wet season and $2.25 \pm 1.61 \text{ m d}^{-1}$ in the dry season). k_{600} during the wet season were also significantly (independent sample t test, $p < 0.05$) higher than the dry season. k_{600} increased 112.7 % and 118.2 % from dry season to wet season in small and large rivers, respectively. However, comparisons

between different phases in the same hydrological period (e.g. early, middle, and late wet season) did not differ significantly (paired sample t test, $p > 0.05$) for both river size classes.

The spatial and temporal variation of CO_2 efflux generally coincided with the changes in $p\text{CO}_2$ and k_{600} since high FCO_2 occurred when k_{600} or $p\text{CO}_2$ were elevated. In small rivers, the highest CO_2 effluxes were $346.8 \pm 625.2 \text{ mmol m}^{-2} \text{ d}^{-1}$ during April, consistent with the high k_{600} and $p\text{CO}_2$ in this period. In large rivers, high CO_2 effluxes were observed in both April ($339.9 \pm 828.6 \text{ mmol m}^{-2} \text{ d}^{-1}$) and August ($329.9 \pm 270.0 \text{ mmol m}^{-2} \text{ d}^{-1}$), which were attributed to high k_{600} in April and high $p\text{CO}_2$ in August.

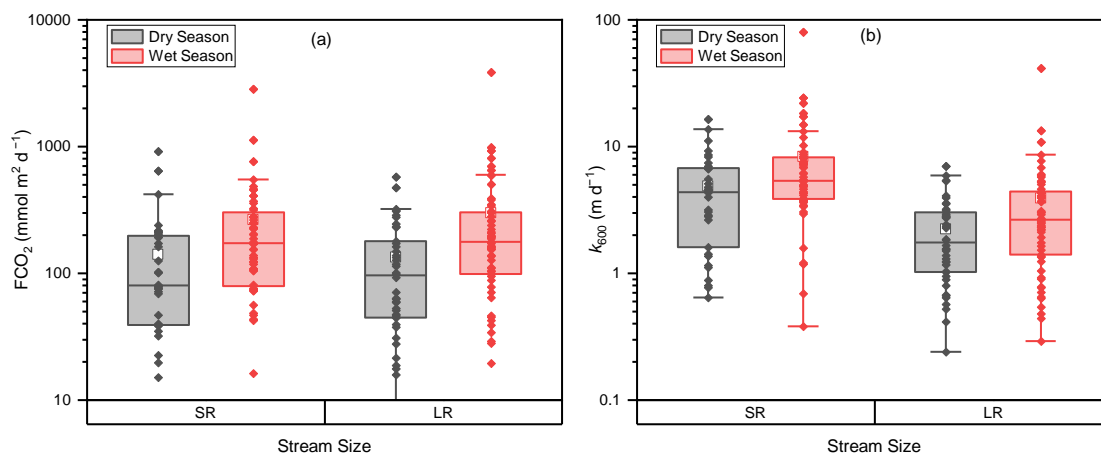


Figure 5 Relationship between stream size and (a) FCO_2 and (b) k_{600} . The box mid-lines represent medians; the interquartile range (IQR) is represented by top and bottom of the box, respectively; whiskers indicate the range of 1.5 IQR; the white square symbols represent means, and the other symbols represent FCO_2 and k_{600} values for each sampled site.

4 Discussions

4.1 Underlying Processes of $p\text{CO}_2$ dynamics

The spatial pattern of $p\text{CO}_2$ in the DJRB is likely resulting from changes in the intensity of in-stream metabolism. Our data showed that river water $p\text{CO}_2$ was negatively related to DO and positively related to DOC (Figure 6), suggesting that metabolic processes are important for CO_2 variation (Amaral et al., 2020). High $p\text{CO}_2$ and low DO in large rivers could result from more favorable conditions for OC composition. Terrestrial organic carbons are difficult to convert into CO_2 in small rivers due to the high flow velocity and short water residence time (Hotchkiss et al., 2015). Conversely, a greater fraction of

OC could be transported and fuel the heterotrophic respiration in large rivers, where low flow velocity
300 and long water residence time facilitated the decomposition of organic carbon within the water column
(Denfeld et al., 2013).

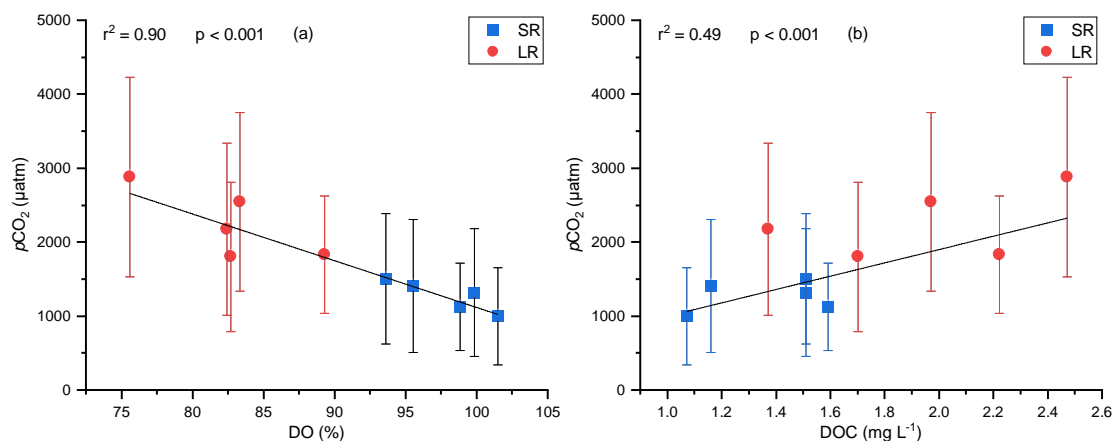


Figure 6 Relationship between seasonal average $p\text{CO}_2$ and (a) DO and (b) DOC. Error bars for the $p\text{CO}_2$ represent 1 standard deviation from the seasonal mean. The DO– $p\text{CO}_2$ and DOC– $p\text{CO}_2$ relationship are shown as solid lines.

305 The spatial pattern of $p\text{CO}_2$ was also related to the variation in carbon input due to different land cover
(Borges et al., 2018). The higher $p\text{CO}_2$ in large rivers than small rivers was associated with a higher
percentage of urban and cropland cover and lower forest cover (Figure S3). Compared with the forest,
cropland could provide a more favorable condition for soil erosion and the transfer of organic matter
from land to rivers, contributing to a higher $p\text{CO}_2$. Intensification of agricultural practices could promote
310 the decomposition of soil organic matter (Borges et al., 2018) and increase the concentration of liable
DOC, which is more sensitive to in-stream metabolism after entering the rivers (Lambert et al., 2017; Li
et al., 2019). Meanwhile, the input of wastewater with high organic matter concentration from the urban
area could also contribute to an increase in riverine $p\text{CO}_2$ (Xuan et al., 2020; Zhang et al., 2021).

Moreover, our result showed increasing $p\text{CO}_2$ from forest-dominated streams in UDJRB to those in
315 agricultural and urban impacted catchments in MDJRB and LDJRB (Figure 3b). Over 70% of forest
cover in UDJRB (Figure 1) can reduce the soil erosion associated with precipitation (Ran et al., 2018).
Meanwhile, the organic matter from forest tend to be more aromatic, thus more capable of surviving
biodegradation (Kalbitz and Kaiser, 2008), leading to a relatively low riverine $p\text{CO}_2$ value. In contrast,
cropland, occupying about 49% of the land cover (Figure 1), was the primary land use type in the MDJRB
320 substituting forest, and urban areas accounting for about 17% of the land cover in the LDJRB. The higher

$p\text{CO}_2$ in the MDJRB and LDJRB is likely under the influence of agricultural practices and wastewater input. Overall, land use mainly affects the spatial distribution of $p\text{CO}_2$ by altering the amount and lability of carbon inputs to the rivers.

325 However, DOC concentration is not likely the primary control of different in-stream metabolism intensities in small and large rivers. Our result showed that large rivers had similar DOC concentration but higher $p\text{CO}_2$ compared with small rivers with similar land cover (Figure 7) when the percentage of forest area was over 65% or the percentage of combined cropland and urban area was less than 30%. This suggested that large rivers have more intense OC decomposition than small rivers with similar DOC concentrations. Therefore, favorable conditions for OC decomposition were more likely to be responsible
330 for the spatial pattern. Another possible carbon source of river water CO_2 is direct soil CO_2 input. However, it is unlikely the major contributor of CO_2 for large rivers in the DJRB, since the contribution of soil CO_2 tends to decrease with the increased stream order and leads to higher $p\text{CO}_2$ in small rivers (Marx et al., 2017), which contradicted with the spatial pattern in this study.

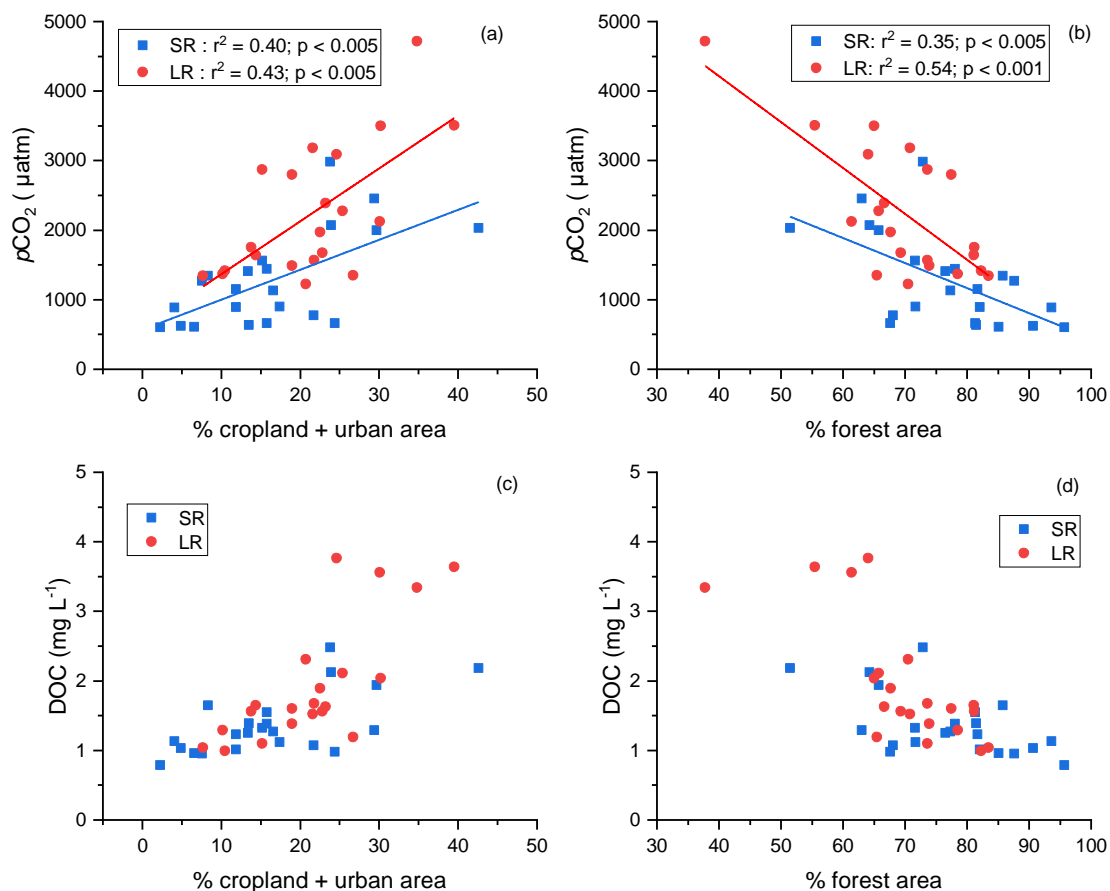


Figure 7 (a) the relationship between yearly average $p\text{CO}_2$ at each site and the percentage of cropland and urban area combined (b) the relationship between yearly average $p\text{CO}_2$ at each site and the percentage of forest area (c) the relationship between yearly average DOC at each site and the percentage of cropland and urban area combined (d) the relationship between yearly average DOC at each site and the percentage of forest area.

On the other hand, the temporal pattern is likely the consequence of changes in terrestrial carbon input and in-stream metabolism intensity. Our result showed that higher $p\text{CO}_2$ occurred in the wet season than the dry season for both small and large rivers (Figure 4). The elevated temperature in the wet season could promote a substantial increase in the net primary productivity of the terrestrial ecosystem, while increased precipitation facilitated the transfer of terrestrial carbon (Rasera et al., 2013), including both soil CO_2 and OC, from land to rivers. This could either enhance riverine $p\text{CO}_2$ directly or by fuelling OC decomposition (Borges et al., 2018). However, differences in seasonal changes of $p\text{CO}_2$ between small and large rivers (Figure 4) also suggested that their primary controlling process could be different. For

small rivers, the highest value of $p\text{CO}_2$ was observed in April (Figure 4), which is consistent with the rapid surge of terrestrial C input, usually occurring at the beginning of the wet season (Hope et al., 2004; Yao et al., 2007; Johnson et al., 2008). However, such an increase in $p\text{CO}_2$ was not observed in large rivers (Figure 4), even though DOC in large rivers, increased during the same period, similar to small
350 rivers (Table 1). A possible explanation is that observed $p\text{CO}_2$ rise was mainly originated from soil CO_2 , which was readily emitted from the small rivers into the air, with little reaching the larger rivers downstream (Denfeld et al., 2013; Drake et al., 2018). Differences in $p\text{CO}_2$ dynamic in July and August also reflected differential controlling processes in small and large rivers. A decline in $p\text{CO}_2$ in July in small rivers suggested that it might have experienced the depletion effect occurring at middle and late
355 wet season (Hope et al., 2004), during which soil CO_2 decreased due to the continual precipitation. In contrast, the increase in $p\text{CO}_2$ occurring in large rivers in July indicated that the decrease in soil CO_2 input could hardly affect the $p\text{CO}_2$ in large rivers during this period. Instead, stronger in-stream metabolism caused by OC input and favorable conditions for OC decomposition is more likely to be responsible for the rising $p\text{CO}_2$.

360 To compare the contribution of internal metabolism on $p\text{CO}_2$ in small and large rivers, ΔCO_2 : ΔO_2 stoichiometry was used to evaluate the impact of respiration and photosynthesis processes on the concentration of O_2 and CO_2 in water bodies (Stets et al., 2017). The inverse relation between ΔCO_2 and ΔO_2 (Figure 8) demonstrated that metabolic processes are important for CO_2 variation (Amaral et al., 2020). It is also supported by the positive relation between river water $p\text{CO}_2$ and DOC and the negative
365 relation between $p\text{CO}_2$ and DO (Figure 6). However, the imbalanced ΔCO_2 : ΔO_2 stoichiometry (Figure 7) indicates that, in addition to in-stream metabolic processes, other factors also affect the CO_2 and O_2 in the water (Stets et al., 2017). For example, 183 out of 215 observations were above the 1:1 ΔCO_2 : ΔO_2 line, suggesting additional sources of carbon input. The difference in the ΔCO_2 : ΔO_2 stoichiometry between small and large rivers reflects their differences in the controlling processes (Rasera et al., 2013).
370 In large rivers, the ΔCO_2 : ΔO_2 stoichiometry is closer to the 1:1 line than in small rivers, suggesting large rivers are more affected by the metabolic processes (Jeffrey et al., 2018; Amaral et al., 2020). In comparison, the deviation from the 1:1 line in small rivers indicates a stronger impact of external carbon sources (Abril et al., 2014; Amaral et al., 2020), which substantiates our finding that $p\text{CO}_2$ of small rivers are more likely affected by soil CO_2 input. Furthermore, there were other processes that could affect the
375 riverine $p\text{CO}_2$. For example, stronger solar radiation during summer could increase photo-oxidation in

380 rivers. However, commonly observed lower daytime CO₂ emission rates than nocturnal rates (Gómez-Gener et al., 2021) suggests that photosynthesis overrides photo-oxidation in CO₂ dynamics. Nonetheless, the low DO concentration observed in the surveyed rivers (Figure 8) suggested that photosynthesis is not the primary control of the seasonal variation of pCO₂.

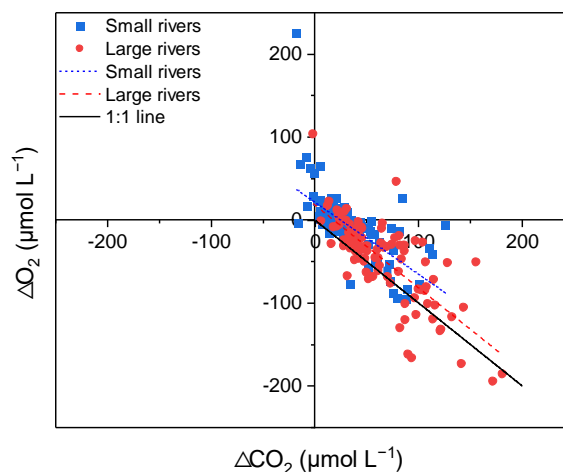
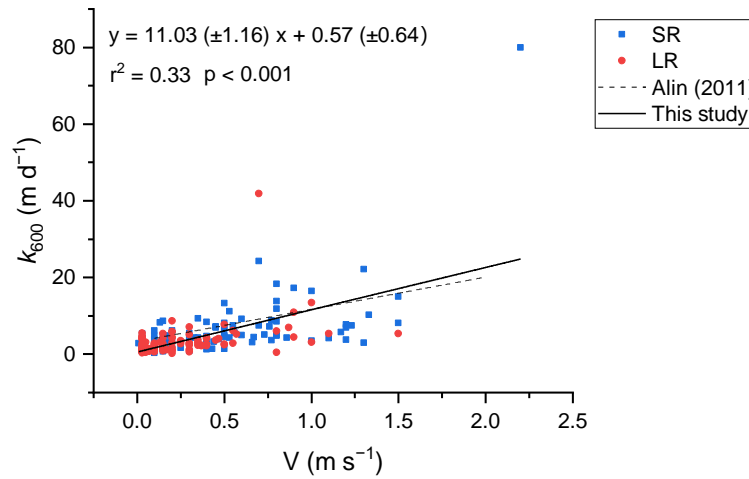


Figure 8 The relationship between ΔCO_2 and ΔO_2 . Points greater than zero are oversaturated, and less than zero are undersaturated. Points above the 1:1 line indicate the existence of additional carbon sources, apart from in-stream metabolic processes.

4.2 Environmental Control of k_{600} variation

385 Environmental factors, including wind speed and hydrological variables, could affect the gas exchange at the water–air interface and were typically used to explain the variance in k_{600} (Alin et al., 2011; Raymond et al., 2012). Flow velocity generally determine the k_{600} in rivers, while wind speed becomes a more important factor in controlling the k_{600} in large rivers, reservoirs and estuary (Guérin et al., 2007; Rasera et al., 2013; Amaral et al., 2020). In our surveyed rivers, k_{600} displayed a significant linear correlation (Pearson correlation, $p < 0.001$) with the flow velocity. Our k_{600} model (Figure 8) base on 188 field measurement data is similar to that developed by Alin et al. (2011) ($k_{600} = 13.82 + 0.35v$).
 390 However, in our studied rivers, no significant correlation (Pearson correlation, $p > 0.05$) was found between wind speed and k_{600} regardless of stream size. This could be explained by the lower wind speed (Table 2, $0.68 \pm 0.66 \text{ m s}^{-1}$ and $1.09 \pm 1.06 \text{ m s}^{-1}$ for small and large rivers, respectively) (Guérin et al.,
 395 2007). As the wind speed decreases, the impact of flow velocity on k_{600} will increase considerably

(Borges et al., 2004). Therefore, the accuracy of k_{600} estimation based on wind speed in nearby regions should be examined using measurement data (Yao et al., 2007; Li et al., 2018). The temporal heterogeneities of k_{600} between small and large rivers reveal the differences in flow regime. k_{600} in small rivers are significantly (independent sample t test, $p < 0.001$) higher than in large rivers, which could be explained by higher flow velocity in small rivers due to a higher gradient. Meanwhile, significantly higher k_{600} (independent sample t test, $p < 0.05$) was also observed in the wet season compared with the dry season, which is the result of increasing flow velocity and turbulence due to plentiful monsoon-induced precipitation during wet season (Guérin et al., 2007; Alin et al., 2011; Ho et al., 2018).



405 **Figure 9** Relationship between k_{600} and flow velocity. The dashed line represents the parameterization of Alin et al (2011).

Table 2. Seasonal variation of k_{600} and environmental factors in small and large rivers.

Stream size	Season	Current velocity (m s ⁻¹)	U10 (m s ⁻¹)	k_{600} (m d ⁻¹)
small	Wet	0.66 ± 0.47	0.62 ± 0.61	8.29 ± 11.29
	Dry	0.43 ± 0.27	0.76 ± 0.73	4.90 ± 3.82
large	Wet	0.32 ± 0.32	0.86 ± 0.91	3.90 ± 5.55
	Dry	0.17 ± 0.19	1.43 ± 1.58	2.25 ± 1.61

Exceptionally high k_{600} values were observed in the surveyed rivers (Figure 9). The highest k_{600} in large and small rivers were 41.83 and 79.97 m d⁻¹, which were 5-fold and 3-fold larger than calculated k_{600} , respectively. This is the result of the exponential increase in k_{600} due to extreme flood events. Generally,

flood events associated with heavy rainfall during the wet season can increase flow velocity and turbulence at the water–air interface (Almeida et al., 2017; Geeraert et al., 2017), leading to substantially higher k_{600} . Yet, neither our model nor the one from Alin et al. (2011) was suitable for the estimation of k_{600} during extreme flood events because the calculated k_{600} could deviate far from the measured k_{600} when they occurred. Therefore, the extent to which flood events affect k_{600} and riverine CO₂ emission is still uncertain and warrant continued research (Drake et al., 2018).

4.3 A Comparison of CO₂ Emissions to Other Rivers

The mean CO₂ fluxes of 225.2 mmol m⁻² d⁻¹ in DJRB is comparable to those observed in tropical and subtropical rivers in the Americas, Africa, and Southeast Asia (Table 3). Although the magnitude of the CO₂ evasion of these river basins is similar, the seasonal variations and drivers behind them could differ. The higher CO₂ emission in the Dongjiang Basin was observed in the wet season compared to the dry season, and this seasonal pattern is similar to that observed in the Xijiang and Daning rivers (Yao et al., 2007; Ni et al., 2019) but different from the one from Jinshui River in the upper reaches of the Yangtze River, where $p\text{CO}_2$ is high in winter and low in summer (Luo et al., 2019), even though all four rivers are in the East Asia Monsoon climate region. The difference in seasonal pattern can be explained by the drivers of $p\text{CO}_2$ variability as the seasonal variation of riverine $p\text{CO}_2$ is likely resulting from the changes of external carbon input, internal production of CO₂ (Yao et al., 2007), and the dilution effect caused by precipitation (Johnson et al., 2007). For rivers where $p\text{CO}_2$ is lower in summer than in winter, the dilution effect overrides the effect of increased carbon inputs and internal CO₂ production (Luo et al., 2019). In contrast, for rivers like the Dongjiang river, although the dilution effect remains, increased CO₂ input and metabolism are more significant factors in controlling $p\text{CO}_2$, thus leading to higher summer $p\text{CO}_2$. In addition, the controlling processes of the Dongjiang River may be different even when compared with rivers with similar seasonal variations in the same climatic zone. For instance, DO in the Xijiang river was supersaturated, indicating that photosynthetic activities in the water body mainly reduce the CO₂ concentration in the rivers (Yao et al., 2007). Therefore, other carbon sources like soil respiration and carbonate weathering should be responsible for high $p\text{CO}_2$ in summer (Zhang et al., 2019). In contrast, low DO value and a negative correlation between DO and $p\text{CO}_2$ have been observed in the Dongjiang River, indicating that photosynthesis is relatively weak compared with the respiration in the water body, and the latter one is an essential source of riverine CO₂ (Stets et al., 2017) resulting in higher $p\text{CO}_2$ in summer.

Table 3. Comparison of CO₂ emission in subtropical and tropical rivers.

Rivers	Climate	Season	pCO ₂ (µatm)	k ₆₀₀ (m d ⁻¹)	FCO ₂ (mmol m ⁻² d ⁻¹)	References
The Dongjiang River (Large rivers)	Subtropical	Wet	2422 ± 1209	3.90 ± 5.55	300.1 ± 511.8	This study
		Dry	1990 ± 1094	2.25 ± 1.61	134.5 ± 129.5	
The Dongjiang River (small rivers)		Wet	1321 ± 792	8.29 ± 11.29	264.2 ± 410.0	
		Dry	1191 ± 825	4.90 ± 3.82	129.5 ± 197.2	
The Xijiang River (Mainstream)	Subtropical		2600		190.3–358.6	(Yao et al., 2007)
The Lower Meikong River	Tropical		1090 ± 290	6.24*	194.5	(Li et al., 2013)
The Yangtze River (Jinshui River)	Subtropical		1147 ± 874	11.1 ± 4.5*	343 ± 413	(Luo et al., 2019)
(headwater stream)		Dry	1562 ± 975		542 ± 477	
		Wet	834 ± 639		192 ± 278	(Ni et al., 2019)
The upper Yangtze River (Daning river)	Subtropical		1198.2 ± 1122.9		329.8 ± 470.2	
		Rainy	1243.7 ± 1111.5	8.1–14.1*	357.4 ± 483.7	
		Dry	1145.5 ± 1146.2	7.0–8.8*	288.7 ± 450.0	
The Zambezi River	Tropical	Wet	3102.5 **	0.05–1.51	350.75	(Teodoru et al., 2014)
		Dry	1150 **		51.92	
The Congo River	Tropical	High water	6001 ± 5008		1149 or 1520	(Borges et al., 2015a; Borges et al., 2015b)
		Low water	4867 ± 2578			
		Falling water	5321 ± 3383			
The Lower Red River	Tropical		1589 ± 43	12.22 ± 6.48	530.3 ± 16.9	(Le et al., 2018)
Caboolture River	Subtropical		3000 ± 33		379 ± 53	(Jeffrey et al., 2018)
Rajang River	Tropical	wet	2531 ± 188	0.55–2.93	141.67	(Müller-Dum et al., 2019)
		dry	2337 ± 304		125	
Lower Mississippi River	Subtropical		1514 ± 652		172.8	(Reiman and Xu, 2019b)
Amazonian Rivers	Tropical		259–7808	5.06	69.12–1321.92	(Rasera et al., 2013)

* *k* values have been showed here because *k*₆₀₀ values were not provided in references; ** the unit for pCO₂ is ppm.

The CO₂ fluxes in small rivers are similar to that in large rivers, which is contradictory to the finding in previous studies that CO₂ effluxes should be higher in small rivers than in large rivers due to the input of CO₂-rich groundwater (Duvert et al., 2018). The depletion and diffusion effect may be responsible for the discrepancy (Johnson et al., 2007; Dinsmore et al., 2013). In the Dongjiang River Basin, groundwater could be easily diluted due to ample monsoon-induced precipitation, preventing it from supplying the small rivers with high concentrations of carbon dioxide. However, we recognize that the impact of groundwater on *p*CO₂ in small rivers may be overlooked in our sampling process since the CO₂ carried by groundwater can emit into the atmosphere within a very short distance (Duvert et al., 2018). In view of the above, it is recommended that further studies targeting the release of groundwater CO₂ to the atmosphere be carried out in the future.

5 Conclusion

Studying CO₂ emissions from subtropical rivers is an essential step toward more accurate estimates of global CO₂ evasion from river systems. By deploying floating chambers, seasonal changes in riverine *p*CO₂ and CO₂ evasion in the Dongjiang river catchment were investigated. Spatial and temporal patterns of *p*CO₂ were mainly affected by terrestrial carbon inputs and in-stream metabolism, both of which varied due to differential catchment settings, land cover, and hydrological conditions. *k*₆₀₀ was higher in small rivers than large rivers and higher during the wet season than the dry season, both of which can be explained by the observed significant correlation between *k*₆₀₀ and the flow velocity. In contrast to previous studies, similar CO₂ fluxes were observed among small and large rivers in the DJRB. It is suggested that the absence of commonly observed higher CO₂ fluxes in small rivers could be associated with the depletion effect caused by abundant and persistent precipitation in this subtropical monsoon catchment. There is no doubt that the spatial and temporal variation of CO₂ evasion in the DJRB reflected the complexity and diversity of controlling factors. As a step towards a more accurate estimate of the carbon budget in the catchment, comprehensive and systematic measurements of CO₂ evasion covering a broad range of stream sizes and seasons are of paramount importance.

Data availability. CO₂ emission data used in this study are available online at: <https://doi.org/10.25442/hku.13416281.v1> (Liu, 2020). Other data are available from the corresponding author Lishan Ran upon request at lsran@hku.hk.

Author contributions. BL and LR conceived the study. BL, MT, CC, XY, and LR carried out the fieldwork. BL, MT, and KS designed and performed the laboratory analysis. BL composed the manuscript with contributions from all authors.

Competing interests. The authors declare that they have no conflict of interest.

475 *Acknowledgements.* This work was financially supported by the Research Grants Council of Hong Kong (Grants: 17300619 and 27300118), the Hui Oi-Chow Trust Fund (Grant: 201801172006) and the National Natural Science Foundation of China (Grant: 41807318).

References

- 480 Abril, G., Martinez, J. M., Artigas, L. F., Moreira-Turcq, P., Benedetti, M. F., Vidal, L., Meziane, T., Kim, J. H., Bernardes, M. C., Savoye, N., Deborde, J., Souza, E. L., Alberic, P., Landim de Souza, M. F., and Roland, F.: Amazon River carbon dioxide outgassing fuelled by wetlands, *Nature*, 505, 395-398, <https://doi.org/10.1038/nature12797>, 2014.
- Abril, G., Bouillon, S., Darchambeau, F., Teodoru, C. R., Marwick, T. R., Tamooh, F., Ochieng Omengo, 485 F., Geeraert, N., Deirmendjian, L., Polsenaere, P., and Borges, A. V.: Technical Note: Large overestimation of $p\text{CO}_2$ calculated from pH and alkalinity in acidic, organic-rich freshwaters, *Biogeosciences*, 12, 67-78, <https://doi.org/10.5194/bg-12-67-201510.5194>, 2015.
- Alin, S. R., Rasera, M. d. F. F. L., Salimon, C. I., Richey, J. E., Holtgrieve, G. W., Krusche, A. V., and Snidvongs, A.: Physical controls on carbon dioxide transfer velocity and flux in low-gradient river 490 systems and implications for regional carbon budgets, *Journal of Geophysical Research*, 116, G01009, <https://doi.org/10.1029/2010jg001398>, 2011.
- Almeida, R. M., Pacheco, F. S., Barros, N., Rosi, E., and Roland, F.: Extreme floods increase CO_2 outgassing from a large Amazonian river, *Limnology and Oceanography*, 62, 989-999, <https://doi.org/10.1002/lno.10480>, 2017.
- 495 Amaral, J. H. F., Melack, J. M., Barbosa, P. M., MacIntyre, S., Kasper, D., Cortés, A., Silva, T. S. F., Nunes de Sousa, R., and Forsberg, B. R.: Carbon dioxide fluxes to the atmosphere from waters within flooded forests in the Amazon basin, *Journal of Geophysical Research: Biogeosciences*, 125, e2019JG005293, <https://doi.org/10.1029/2019JG005293>, 2020.
- Battin, T. J., Luyssaert, S., Kaplan, L. A., Aufdenkampe, A. K., Richter, A., and Tranvik, L. J.: The 500 boundless carbon cycle, *Nature Geoscience*, 2, 598-600, <https://doi.org/10.1038/ngeo618>, 2009.
- Borges, A. V., Delille, B., Schiettecatte, L. S., Gazeau, F., Abril, G., Frankignoulle, M. J. L., and Oceanography: Gas transfer velocities of CO_2 in three European estuaries (Randers Fjord, Scheldt, and Thames), *Limnology Oceanography*, 49, 1630-1641, <https://doi.org/10.4319/lo.2004.49.5.1630>, 2004.
- Borges, A. V., Abril, G., Darchambeau, F., Teodoru, C. R., Deborde, J., Vidal, L. O., Lambert, T., and 505 Bouillon, S.: Divergent biophysical controls of aquatic CO_2 and CH_4 in the World's two largest rivers, *Scientific Reports*, 5, 15614, 10.1038/srep15614, 2015a.
- Borges, A. V., Darchambeau, F., Teodoru, C. R., Marwick, T. R., Tamooh, F., Geeraert, N., Omengo, F. O., Guérin, F., Lambert, T., Morana, C., Okuku, E., and Bouillon, S.: Globally significant greenhouse-gas emissions from African inland waters, *Nature Geoscience*, 8, 637-642, 10.1038/ngeo2486, 2015b.
- 510 Borges, A. V., Darchambeau, F., Lambert, T., Bouillon, S., Morana, C., Brouyere, S., Hakoun, V., Jurado, A., Tseng, H. C., Descy, J. P., and Roland, F. A. E.: Effects of agricultural land use on fluvial carbon dioxide, methane and nitrous oxide concentrations in a large European river, the Meuse (Belgium), *Science of The Total Environment*, 610-611, 342-355, <https://doi.org/10.1016/j.scitotenv.2017.08.047>, 2018.
- 515 Chen, Q., Xu, W., Li, S., Fu, S., and Yan, J.: Aboveground biomass and corresponding carbon sequestration ability of four major forest types in south China, *Chinese Science Bulletin*, 58, 1551-1557, 10.1007/s11434-012-5100-8, 2013.
- Chen, Y. D., Zhang, Q., Lu, X., Zhang, S., and Zhang, Z.: Precipitation variability (1956–2002) in the Dongjiang River (Zhujiang River basin, China) and associated large-scale circulation, *Quaternary 520 International*, 244, 130-137, <https://doi.org/10.1016/j.quaint.2010.08.013>, 2011.
- Cole, J. J., Prairie, Y. T., Caraco, N. F., McDowell, W. H., Tranvik, L. J., Striegl, R. G., Duarte, C. M., Kortelainen, P., Downing, J. A., Middelburg, J. J., and Melack, J.: Plumbing the global carbon cycle: Integrating inland waters into the terrestrial carbon budget, *Ecosystems*, 10, 172-185,

- <https://doi.org/10.1007/s10021-006-9013-8>, 2007.
- 525 Denfeld, B. A., Frey, K. E., Sobczak, W. V., Mann, P. J., and Holmes, R. M.: Summer CO₂ evasion from streams and rivers in the Kolyma River basin, north-east Siberia, *Polar Research*, 32, 19704, <https://doi.org/10.3402/polar.v32i0.19704>, 2013.
- Dickson, A. G., Sabine, C. L., and Christian, J. R.: Guide to best practices for ocean CO₂ measurements, North Pacific Marine Science Organization, 2007.
- 530 Ding, J., Jiang, Y., Fu, L., Liu, Q., Peng, Q., and Kang, M.: Impacts of land use on surface water quality in a subtropical river basin: A case study of the Dongjiang River Basin, Southeastern China, *Water*, 7, 4427-4445, <https://doi.org/10.3390/w7084427>, 2015.
- Dinsmore, K. J., Wallin, M. B., Johnson, M. S., Billett, M. F., Bishop, K., Pumpanen, J., and Ojala, A.: Contrasting CO₂ concentration discharge dynamics in headwater streams: A multi-catchment comparison, *Journal of Geophysical Research: Biogeosciences*, 118, 445-461, <https://doi.org/10.1002/jgrg.20047>, 2013.
- 535 Drake, T. W., Raymond, P. A., and Spencer, R. G.: Terrestrial carbon inputs to inland waters: A current synthesis of estimates and uncertainty, *Limnology and Oceanography Letters*, 3, 132-142, <https://doi.org/10.1002/lol2.10055>, 2018.
- 540 Duvert, C., Butman, D. E., Marx, A., Ribolzi, O., and Hutley, L. B.: CO₂ evasion along streams driven by groundwater inputs and geomorphic controls, *Nature Geoscience*, 11, 813-818, <https://doi.org/10.1038/s41561-018-0245-y>, 2018.
- Fu, Y., Tang, C., Li, J., Zhao, Y., Zhong, W., and Zeng, X.: Sources and transport of organic carbon from the Dongjiang River to the Humen outlet of the Pearl River, southern China, *Journal of Geographical Sciences*, 24, 143-158, <https://doi.org/10.1007/s11442-014-1078-2>, 2014.
- 545 Geeraert, N., Omengo, F. O., Borges, A. V., Govers, G., and Bouillon, S.: Shifts in the carbon dynamics in a tropical lowland river system (Tana River, Kenya) during flooded and non-flooded conditions, *Biogeochemistry*, 132, 141-163, <https://doi.org/10.1007/s10533-017-0292-2>, 2017.
- Gómez-Gener, L., Rocher-Ros, G., Battin, T., Cohen, M. J., Dalmagro, H. J., Dinsmore, K. J., Drake, T. W., Duvert, C., Enrich-Prast, A., Horgby, Å., Johnson, M. S., Kirk, L., Machado-Silva, F., Marzolf, N. S., McDowell, M. J., McDowell, W. H., Miettinen, H., Ojala, A. K., Peter, H., Pumpanen, J., Ran, L., Riveros-Iregui, D. A., Santos, I. R., Six, J., Stanley, E. H., Wallin, M. B., White, S. A., and Sponseller, R. A.: Global carbon dioxide efflux from rivers enhanced by high nocturnal emissions, *Nature Geoscience*, 10.1038/s41561-021-00722-3, 2021.
- 555 Guérin, F., Abril, G., Serça, D., Delon, C., Richard, S., Delmas, R., Tremblay, A., and Varfalvy, L.: Gas transfer velocities of CO₂ and CH₄ in a tropical reservoir and its river downstream, *Journal of Marine Systems*, 66, 161-172, <https://doi.org/10.1016/j.jmarsys.2006.03.019>, 2007.
- Ho, D. T., Engel, V. C., Ferrón, S., Hickman, B., Choi, J., and Harvey, J. W.: On factors influencing air - water gas exchange in emergent wetlands, *Journal of Geophysical Research: Biogeosciences*, 123, 178-192, <https://doi.org/10.1002/2017JG004299>, 2018.
- 560 Hope, D., Billett, M., and Cresser, M.: A review of the export of carbon in river water: fluxes and processes, *Environmental Pollution*, 84, 301-324, 1994.
- Hope, D., Palmer, S. M., Billett, M. F., and Dawson, J. J. H. P.: Variations in dissolved CO₂ and CH₄ in a first - order stream and catchment: an investigation of soil-stream linkages, *Journal of Hydrological Processes*, 18, 3255-3275, <https://doi.org/10.1002/hyp.5657>, 2004.
- 565 Hotchkiss, E., Hall Jr, R., Sponseller, R., Butman, D., Klaminder, J., Laudon, H., Rosvall, M., and Karlsson, J. J. N. G.: Sources of and processes controlling CO₂ emissions change with the size of streams and rivers, *Nature Geoscience*, 8, 696-699, <https://doi.org/10.1038/ngeo2507>, 2015.
- Jeffrey, L. C., Santos, I. R., Tait, D. R., Makings, U., and Maher, D. T.: Seasonal drivers of carbon dioxide

- 570 dynamics in a hydrologically modified subtropical tidal river and estuary (Caboolture River, Australia),
Journal of Geophysical Research: Biogeosciences, 123, 1827-1849,
<https://doi.org/10.1029/2017jg004023>, 2018.
- Johnson, M. S., Weiler, M., Couto, E. G., Riha, S. J., and Lehmann, J.: Storm pulses of dissolved CO₂ in
a forested headwater Amazonian stream explored using hydrograph separation, Water resources research,
575 43, <https://doi.org/10.1029/2007WR006359>, 2007.
- Johnson, M. S., Lehmann, J., Riha, S. J., Krusche, A. V., Richey, J. E., Ometto, J. P. H., and Couto, E.
G.: CO₂ efflux from Amazonian headwater streams represents a significant fate for deep soil respiration,
Geophysical Research Letters, 35, <https://doi.org/10.1029/2008GL034619>, 2008.
- 580 Kalbitz, K., and Kaiser, K.: Contribution of dissolved organic matter to carbon storage in forest mineral
soils, Journal of Plant Nutrition and Soil Science, 171, 52-60, <https://doi.org/10.1002/jpln.200700043>,
2008.
- Lambert, T., Bouillon, S., Darchambeau, F., Morana, C., Roland, F. A. E., Descy, J.-P., and Borges, A. V.:
Effects of human land use on the terrestrial and aquatic sources of fluvial organic matter in a temperate
river basin (The Meuse River, Belgium), Biogeochemistry, 136, 191-211, 10.1007/s10533-017-0387-9,
585 2017.
- Lauerwald, R., Laruelle, G. G., Hartmann, J., Ciais, P., and Regnier, P. A.: Spatial patterns in CO₂ evasion
from the global river network, Global Biogeochemical Cycles, 29, 534-554,
<https://doi.org/10.1002/2014GB004941>, 2015.
- Le Coz, J., Pierrefeu, G., and Paquier, A.: Evaluation of river discharges monitored by a fixed side-
590 looking Doppler profiler, Water Resources Research, 44, <https://doi.org/10.1029/2008WR006967>, 2008.
- Le, T. P. Q., Marchand, C., Ho, C. T., Da Le, N., Duong, T. T., Lu, X., Doan, P. K., Nguyen, T. K., Nguyen,
T. M. H., and Vu, D. A.: CO₂ partial pressure and CO₂ emission along the lower Red River (Vietnam),
Biogeosciences, 15, 4799-4814, <https://doi.org/10.5194/bg-15-4799-2018>, 2018.
- 600 Li, S., Lu, X. X., and Bush, R. T.: CO₂ partial pressure and CO₂ emission in the Lower Mekong River,
Journal of Hydrology, 504, 40-56, <https://doi.org/10.1016/j.jhydrol.2013.09.024>, 2013.
- Li, S., Ni, M., Mao, R., and Bush, R. T.: Riverine CO₂ supersaturation and outgassing in a subtropical
monsoonal mountainous area (Three Gorges Reservoir Region) of China, Journal of Hydrology, 558,
460-469, <https://doi.org/10.1016/j.jhydrol.2018.01.057>, 2018.
- Li, X., Xu, J., Shi, Z., and Li, R.: Response of Bacterial Metabolic Activity to the River Discharge in the
605 Pearl River Estuary: Implication for CO₂ Degassing Fluxes, Frontiers in Microbiology, 10,
10.3389/fmicb.2019.01026, 2019.
- Liang, B., Hu, J. T., Li, S. Y., Ye, Y. X., Liu, D. H., and Huang, J.: Carbon system simulation in the Pearl
River Estuary, China: Mass fluxes and transformations, Journal of Geophysical Research:
Biogeosciences, 125, e2019JG005012, <https://doi.org/10.1029/2019jg005012>, 2020.
- 605 Luo, J., Li, S., Ni, M., and Zhang, J.: Large spatiotemporal shifts of CO₂ partial pressure and CO₂
degassing in a monsoonal headwater stream, Journal of Hydrology, 579, 124135,
<https://doi.org/10.1016/j.jhydrol.2019.124135>, 2019.
- Marx, A., Dusek, J., Jankovec, J., Sanda, M., Vogel, T., van Geldern, R., Hartmann, J., and Barth, J. A.
C.: A review of CO₂ and associated carbon dynamics in headwater streams: A global perspective,
610 Reviews of Geophysics, 55, 560-585, <https://doi.org/10.1002/2016rg000547>, 2017.
- Millero, F. J., Graham, T. B., Huang, F., Bustos-Serrano, H., and Pierrot, D.: Dissociation constants of
carbonic acid in seawater as a function of salinity and temperature, Marine Chemistry, 100, 80-94,
<https://doi.org/10.1016/j.marchem.2005.12.001>, 2006.
- Moramarco, T., Saltalippi, C., and Singh, V. P.: Estimation of Mean Velocity in Natural Channels Based
615 on Chiu's Velocity Distribution Equation, Journal of Hydrologic Engineering, 9, 42-50,

- doi:10.1061/(ASCE)1084-0699(2004)9:1(42), 2004.
- Müller-Dum, D., Warneke, T., Rixen, T., Müller, M., Baum, A., Christodoulou, A., Oakes, J., Eyre, B. D., and Notholt, J.: Impact of peatlands on carbon dioxide (CO₂) emissions from the Rajang River and Estuary, Malaysia, *Biogeosciences*, 16, 17-32, <https://doi.org/10.5194/bg-16-17-2019>, 2019.
- 620 Ni, M., Li, S., Luo, J., and Lu, X.: CO₂ partial pressure and CO₂ degassing in the Daning River of the upper Yangtze River, China, *Journal of Hydrology*, 569, 483-494, <https://doi.org/10.1016/j.jhydrol.2018.12.017>, 2019.
- Ran, L., Lu, X. X., Yang, H., Li, L., Yu, R., Sun, H., and Han, J.: CO₂ outgassing from the Yellow River network and its implications for riverine carbon cycle, *Journal of Geophysical Research: Biogeosciences*, 625 120, 1334-1347, <https://doi.org/10.1002/2015jg002982>, 2015.
- Ran, L., Li, L., Tian, M., Yang, X., Yu, R., Zhao, J., Wang, L., and Lu, X.: Riverine CO₂ emissions in the Wuding River catchment on the Loess Plateau: Environmental controls and dam impoundment impact, *Journal of Geophysical Research: Biogeosciences*, 122, 1439-1455, <https://doi.org/10.1002/2016JG003713>, 2017a.
- 630 Ran, L., Lu, X. X., and Liu, S.: Dynamics of riverine CO₂ in the Yangtze River fluvial network and their implications for carbon evasion, *Biogeosciences*, 14, 2183-2198, <https://doi.org/10.5194/bg-14-2183-2017>, 2017b.
- Ran, L., Lu, X., Fang, N., and Yang, X.: Effective soil erosion control represents a significant net carbon sequestration, *Scientific reports*, 8, 12018, 2018.
- 635 Ran, Y., Li, X., Lu, L., and Li, Z.: Large-scale land cover mapping with the integration of multi-source information based on the Dempster-Shafer theory, *International Journal of Geographical Information Science*, 26, 169-191, 2012.
- Rasera, M. d. F. F., Krusche, A. V., Richey, J. E., Ballester, M. V., and Victoria, R. L.: Spatial and temporal variability of pCO₂ and CO₂ efflux in seven Amazonian Rivers, *Biogeochemistry*, 116, 241-259, 640 <https://doi.org/10.1007/s10533-013-9854-0>, 2013.
- Raymond, P. A., Zappa, C. J., Butman, D., Bott, T. L., Potter, J., Mulholland, P., Laursen, A. E., McDowell, W. H., and Newbold, D.: Scaling the gas transfer velocity and hydraulic geometry in streams and small rivers, *Limnology and Oceanography: Fluids and Environments*, 2, 41-53, <https://doi.org/10.1215/21573689-1597669>, 2012.
- 645 Raymond, P. A., Hartmann, J., Lauerwald, R., Sobek, S., McDonald, C., Hoover, M., Butman, D., Striegl, R., Mayorga, E., and Humborg, C.: Global carbon dioxide emissions from inland waters, *Nature*, 503, 355-359, <https://doi.org/10.1038/nature12760>, 2013.
- Reiman, J. H., and Xu, Y. J.: Diel Variability of pCO₂ and CO₂ Outgassing from the Lower Mississippi River: Implications for Riverine CO₂ Outgassing Estimation, *Water*, 11, 43, 2019a.
- 650 Reiman, J. H., and Xu, Y. J.: Dissolved carbon export and CO₂ outgassing from the lower Mississippi River – Implications of future river carbon fluxes, *Journal of Hydrology*, 578, 124093, <https://doi.org/10.1016/j.jhydrol.2019.124093>, 2019b.
- Sawakuchi, H. O., Neu, V., Ward, N. D., Barros, M. d. L. C., Valerio, A. M., Gagne-Maynard, W., Cunha, A. C., Less, D. F. S., Diniz, J. E. M., Brito, D. C., Krusche, A. V., and Richey, J. E.: Carbon dioxide emissions along the lower Amazon River, *Frontiers in Marine Science*, 4, 655 <https://doi.org/10.3389/fmars.2017.00076>, 2017.
- Stets, E. G., Butman, D., McDonald, C. P., Stackpoole, S. M., DeGrandpre, M. D., and Striegl, R. G.: Carbonate buffering and metabolic controls on carbon dioxide in rivers, *Global Biogeochemical Cycles*, 31, 663-677, <https://doi.org/10.1002/2016gb005578>, 2017.
- 660 Tao, Z., Gao, Q., Wang, Z., Zhang, S., Xie, C., Lin, P., Ruan, X., Li, S., and Mao, H.: Estimation of carbon sinks in chemical weathering in a humid subtropical mountainous basin, *Chinese Science Bulletin*,

- 56, 3774-3782, <https://doi.org/10.1007/s11434-010-4318-6>, 2011.
- Teodoru, C., Nyoni, F., Borges, A., Darchambeau, F., Nyambe, I., and Bouillon, S.: Spatial variability and temporal dynamics of greenhouse gas (CO₂, CH₄, N₂O) concentrations and fluxes along the Zambezi River mainstem and major tributaries, *Biogeosciences Discussion*, 11, 16391-16445, <https://doi.org/10.5194/bgd-11-16391-2014>, 2014.
- 665 Tian, M., Yang, X., Ran, L., Su, Y., Li, L., Yu, R., Hu, H., and Lu, X. X.: Impact of land cover types on riverine CO₂ outgassing in the Yellow River source region, *Water*, 11, 2243, <https://doi.org/10.3390/w11112243>, 2019.
- 670 Wanninkhof, R.: Relationship between wind speed and gas exchange over the ocean, *Journal of Geophysical Research: Oceans*, 97, 7373-7382, <https://doi.org/10.1029/92JC00188>, 1992.
- Weiss, R. F.: Carbon dioxide in water and seawater: the solubility of a non-ideal gas, *Marine Chemistry*, 2, 203-215, [https://doi.org/10.1016/0304-4203\(74\)90015-2](https://doi.org/10.1016/0304-4203(74)90015-2), 1974.
- 675 Xuan, Y., Cao, Y., Tang, C., and Li, M.: Changes in dissolved inorganic carbon in river water due to urbanization revealed by hydrochemistry and carbon isotope in the Pearl River Delta, China, *Environmental Science and Pollution Research*, 10.1007/s11356-020-08454-4, 2020.
- Yao, G., Gao, Q., Wang, Z., Huang, X., He, T., Zhang, Y., Jiao, S., and Ding, J.: Dynamics of CO₂ partial pressure and CO₂ outgassing in the lower reaches of the Xijiang River, a subtropical monsoon river in China, *Science of The Total Environment*, 376, 255-266, <https://doi.org/10.1016/j.scitotenv.2007.01.080>,
- 680 2007.
- Zhang, L., Qin, X., Liu, P., Huang, Q., Lan, F., and Ji, H.: Estimation of carbon sink fluxes in the Pearl River basin (China) based on a water-rock-gas-organism interaction model, *Environmental Earth Sciences*, 74, 945-952, <https://doi.org/10.1007/s12665-014-3788-2>, 2015.
- 685 Zhang, S., Lu, X. X., Higgitt, D. L., Chen, C.-T. A., Han, J., and Sun, H.: Recent changes of water discharge and sediment load in the Zhujiang (Pearl River) Basin, China, *Global and Planetary Change*, 60, 365-380, <https://doi.org/10.1016/j.gloplacha.2007.04.003>, 2008.
- Zhang, T., Li, J., Pu, J., and Yuan, D.: Carbon dioxide exchanges and their controlling factors in Guijiang River, SW China, *Journal of Hydrology*, 578, 124073, <https://doi.org/10.1016/j.jhydrol.2019.124073>, 2019.
- 690 Zhang, W., Li, H., Xiao, Q., and Li, X.: Urban rivers are hotspots of riverine greenhouse gas (N₂O, CH₄, CO₂) emissions in the mixed-landscape chaohu lake basin, *Water Research*, 189, 116624, <https://doi.org/10.1016/j.watres.2020.116624>, 2021.